Boundary-Layer Meteorol
DOI 10.1007/s10546-015-0047-3

ARTICLE

Quantifying the Influence of Random Errors in Turbulence Measurements on Scalar Similarity in the Atmospheric Surface Layer

Kang Sun[1,2] · Dan Li[3] · Lei Tao[1,2] · Zhongkuo Zhao[4,5] · Mark A. Zondlo[1,2]

Received: 31 October 2014 / Accepted: 21 May 2015

Abstract The influence of random errors in turbulence measurements on scalar similarity for temperature, water vapour, CO_2, and NH_3 is investigated using two eddy-covariance datasets collected over a lake and a cattle feedlot. Three measures of scalar similarity, namely, the similarity constant in the flux–variance relationship, the correlation coefficient between two scalars and the relative transport efficiency, are examined. The uncertainty in the similarity constant C_s in the flux–variance relationship resulting from random errors in turbulence measurements is quantified based on error propagation analyses and a Monte-Carlo sampling method, which yields a distribution instead of a single value for C_s. For different scalars, the distributions of C_s are found to significantly overlap, implying that scalars are transported similarly under strongly unstable conditions. The random errors in the correlation coefficients between scalars and the relative transport efficiencies are also quantified through error propagation analyses, and they increase as the atmosphere departs from neutral conditions. Furthermore, the correlation coefficients between three scalars (water vapour, CO_2, and NH_3) are statistically different from unity while the relative transport efficiencies are not, which highlights the difference between these two measures of scalar similarity. The results suggest that uncertainties in these measures of scalar similarity need to be quantified when using them to diagnose the existence of dissimilarity among different scalars.

✉ Dan Li
danl@princeton.edu

1 Department of Civil and Environmental Engineering, Princeton University, Princeton, NJ 08544, USA

2 Center for Mid-Infrared Technologies for Health and the Environment, NSF-ERC, Princeton, NJ 08544, USA

3 Program of Atmospheric and Oceanic Sciences, Princeton University, Princeton, NJ 08544, USA

4 Institute of Tropical and Marine Meteorology/Guangdong Provincial Key Laboratory of Regional Numerical Weather Prediction, China Meteorology Administration, Guangzhou, China

5 State Key Laboratory of Severe Weather, Chinese Academy of Meteorological Sciences, Beijing, China

Published online: 04 June 2015

Keywords Eddy-covariance fluxes · Flux–variance relationship · Monin–Obukhov similarity · Random errors · Scalar similarity

1 Introduction

It is usually assumed that all scalars, such as temperature, water vapour and trace gases (e.g., CO_2, NH_3, and CH_4) are transported similarly by turbulent flows in the atmospheric boundary layer (ABL). This assumption has important implications in atmospheric sciences, hydrology, ecology and many other disciplines (Stull 1988). For example, turbulent diffusivities for heat and water vapour are usually assumed to be identical in numerical models (Stensrud 2007). This assumption is also important when deriving Penman's equation for evaporation (Brutsaert 1982). Assuming similarity between turbulent transport of trace gases (e.g., CO_2, NH_3, and CH_4) and temperature also allows one to apply the turbulent diffusivity for heat, which is relatively easy to quantify, to estimate fluxes of these trace gases from their mean profiles. Given that high frequency measurements of most trace gases are not widely available, the validation of this assumption is critically needed to quantify the fluxes of greenhouse gases and air pollutants, which are crucial for better understanding climate change (Shindell et al. 2009) and air quality (Martin et al. 2004).

In the atmospheric surface layer (ASL), typically defined as the lowest 10–15 % of the ABL (Stull 1988), the Monin–Obukhov similarity theory (MOST, Monin and Obukhov 1954) is often used to investigate the statistical relationships in turbulent flows, such as flux–profile relationships and flux–variance relationships. According to MOST, these relationships are only functions of the stability parameter, z/L, where z is the height above the ground surface and L is the Obukhov length scale defined as $L = -\frac{u_*^3 \overline{\theta_v}}{\kappa g \overline{w'\theta_v'}}$, where u_* is the friction velocity, θ_v is the surface virtual potential temperature, κ is the von Karman constant, g is the acceleration due to gravity ($= 9.81\ \mathrm{m\ s^{-2}}$), w is the vertical wind speed, and $\overline{w'\theta_v'}$ is the surface buoyancy flux. The overbar denotes the ensemble average (which is approximated by the time average over a 30-min period in this study), and the prime denotes excursions from this average.

Following MOST, it can be derived theoretically that temperature and water vapour are transported similarly (Hill 1989; Dias 2013), and it is not surprising to see that this assumption is often extended to other scalars such as trace gases. However, several assumptions central to MOST break down under certain conditions, which may then induce dissimilarity among different scalars (Dias and Brutsaert 1996; McNaughton and Laubach 1998; Sempreviva and Hojstrup 1998; De Bruin et al. 1999; Lee et al. 2004; Asanuma et al. 2007; Assouline et al. 2008; Detto et al. 2008; Katul et al. 2008; Moene and Schuttemeyer 2008; Li et al. 2012). Key assumptions for MOST include stationarity, horizontal homogeneity, and a sufficiently high Reynolds number (Monin and Obukhov 1954). As such, when non-stationarity (McNaughton and Laubach 1998), advection (Lee et al. 2004), surface heterogeneity (Williams et al. 2007; Moene and Schuttemeyer 2008), and outer-layer influences on the ASL (Asanuma et al. 2007; Katul et al. 2008; Li et al. 2012) are prominent, scalar dissimilarity is often observed, which can be manifest in various similarity functions such as flux–profile relationships and flux–variance relationships (also see Li et al. 2012 for scalar dissimilarity in flux–structure parameter relationships). In this study, we focus on flux–variance relationships due to their widespread use and relation to correlation coefficients between the vertical velocity and the scalar concentrations (R_{ws}, where s denotes the scalar concentration), which are usually used to indicate turbulent transport efficiencies (Dias 2013).

The flux–variance relationship of a scalar s is defined as $\sigma_s/|s_*|$, where σ_s is the standard deviation of the scalar concentration and $s_* = \overline{w's'}/u_*$ is the surface scalar scaling parame-

ter ($\overline{w's'}$ is the scalar flux). Flux–variance relationships have a well-established asymptotic behaviour under free convective conditions ($-z/L \to \infty$), where buoyancy-generated turbulence dominates over shear-generated turbulence. Under these conditions, u_* is no longer a relevant scale in dimensional arguments. As a result, flux–variance relationships follow a '–1/3' power-law scaling,

$$\frac{\sigma_s}{|s_*|} = C_s \left(-\frac{z}{L}\right)^{-\frac{1}{3}}, \tag{1}$$

where C_s is a similarity constant. This asymptotic behaviour has been verified extensively in experimental studies (Monin and Yaglom 1975) and is even used as a quality control for eddy-covariance datasets (Zhao et al. 2013). It is easy to show that for two scalars (s and t), $C_s/C_t = R_{wt}/R_{ws}$. That is, the ratio of similarity constants in flux–variance relationships (C_s/C_t) is identical to the inverse of the relative turbulent transport efficiency (R_{wt}/R_{ws}).

Traditionally, C_s is determined by linear regression between measured $\sigma_s/|s_*|$ and $(-z/L)^{-1/3}$ over a range of strongly unstable conditions. Different values of C_s were reported in the literature for different scalars and the differences in C_s were used as a proof of scalar dissimilarity (Asanuma and Brutsaert 1999; Assouline et al. 2008; Hsieh et al. 2008). The difference in C_s between different scalars can certainly arise from violations of key assumptions in MOST and in this case, any difference in C_s is indeed a proof of scalar dissimilarity. For example, Cava et al. (2008) showed that the entrainment from the top of the ABL affects the turbulent transport of heat in the ASL and induces scalar dissimilarity. However, it is also possible that part of the variability associated with C_s is related to uncertainties in turbulence measurements arising from instrument errors and random errors due to time averaging over an insufficient period for the temporal mean to converge to the ensemble mean (Lumley and Panofsky 1964).

Quantifying uncertainties in C_s induced by different errors in turbulence measurements is important for rigorously assessing scalar similarity or dissimilarity. Nonetheless, these uncertainties are usually not reported in the literature, and there are few discussions on how these uncertainties might affect the results in terms of scalar similarity. One important aim of the present study is to quantify the influence of random errors, which are considered to be the major source of uncertainties in ASL turbulence measurements (Salesky and Chamecki 2012), on the similarity constant C_s. In addition, the impacts of random errors on another two measures of scalar similarity, the correlation coefficient between two scalars (R_{st}) and the relative turbulent transport efficiency (R_{ws}/R_{wt}), are also examined.

An important aspect of our study is the inclusion of four simultaneously measured scalars, namely temperature, water vapour, CO_2 and NH_3 concentrations. To our knowledge, this is the first time that turbulent transport of NH_3 in the ASL has been studied in the context of scalar similarity, which is enabled through a recently developed quantum cascade (QC) laser-based sensor that measures the NH_3 concentration at high frequency (Miller et al. 2014; Sun et al. 2014). We also use data collected from two vastly different field sites, a lake (Bou-Zeid et al. 2008; Li and Bou-Zeid 2011) and a cattle feedlot. The comparisons among multiple scalars and between two datasets allow us to generalize our conclusions.

2 Methodology

2.1 Deriving Random Errors Using Error Propagation

The filtering method proposed by Salesky et al. (2012) is adopted here to estimate random errors in turbulent fluxes and variances. This method has the advantage of not requiring an a

priori estimate of the integral time scale, which itself is subject to large uncertainties (Salesky et al. 2012). The filtering method cannot be directly applied to variables that are functions of turbulent fluxes and/or variances. The random errors in these variables are derived using an error propagation relation (Salesky and Chamecki 2012),

$$\delta_z^2 \approx \delta_x^2 \left(\frac{\partial z}{\partial x}\right)^2 + \delta_y^2 \left(\frac{\partial z}{\partial y}\right)^2 + 2\mathrm{Cov}(x, y)\frac{\partial z}{\partial x}\frac{\partial z}{\partial y}, \tag{2}$$

where z is a function of x and y, and δ_z denotes the random error in z. $\mathrm{Cov}(x, y)$ is the covariance between the random errors in x and y. Following Salesky and Chamecki (2012), we also assume these covariances are zero and it is not clear to us how these covariances can be estimated for each 30-min segment. As can be seen from Eq. 1, the random errors in the standard deviation of scalar s, the dimensionless scalar flux s_*, and the stability parameter z/L need to be quantified in order to estimate the uncertainties associated with C_s. The standard deviation of scalar s can be written as $\sigma_s = \left(\overline{s's'}\right)^{\frac{1}{2}}$, so its random error, δ_{σ_s}, can be quantified as

$$\delta_{\sigma_s} = \frac{1}{2}\delta_{\overline{s's'}}\left(\overline{s's'}\right)^{-\frac{1}{2}}, \tag{3}$$

where $\delta_{\overline{s's'}}$ is the random error in the variance of scalar concentration, which can be estimated using the filtering method (Salesky et al. 2012). The random error in the dimensionless scalar flux s_* can be calculated from

$$\delta_{s_*} \approx \left[\delta_{\overline{w's'}}^2\left(\frac{1}{u_*}\right)^2 + \delta_{u_*}^2\left(\frac{-\overline{w's'}}{{u_*}^2}\right)^2\right]^{\frac{1}{2}} = \left[\frac{\delta_{\overline{w's'}}^2 {u_*}^2 + \delta_{u_*}^2 \overline{w's'}^2}{{u_*}^4}\right]^{\frac{1}{2}}, \tag{4}$$

where $\delta_{u_*} = \frac{1}{2u_*^3}\left(\delta_{\overline{u'w'}}^2 \overline{u'w'}^2 + \delta_{\overline{v'w'}}^2 \overline{v'w'}^2\right)^{\frac{1}{2}}$ is the random error in the friction velocity given by Salesky and Chamecki (2012). The random error in the dimensionless standard deviation $\sigma_s/|s_*|$ follows

$$\delta_{\frac{\sigma_s}{s_*}} \approx \left[\delta_{\sigma_s}^2\left(\frac{1}{s_*}\right)^2 + \delta_{s_*}^2\left(\frac{-\sigma_s}{{s_*}^2}\right)^2\right]^{\frac{1}{2}} = \left[\frac{\delta_{\sigma_s}^2 s_*^2 + \delta_{s_*}^2 \sigma_s^2}{{s_*}^4}\right]^{\frac{1}{2}}, \tag{5}$$

and the random error in z/L is

$$\delta_{z/L} \approx \left[\delta_{u_*}^2\left(\frac{\partial z/L}{\partial u_*}\right)^2 + \delta_{\overline{w'\theta'}}^2\left(\frac{\partial z/L}{\partial \overline{w'\theta'}}\right)^2\right]^{1/2}. \tag{6}$$

As mentioned in the Sect. 1, correlation coefficients are also widely used to indicate scalar similarity, and their random errors are quantified herein. The correlation coefficient between two scalars s and t can be written as $R_{st} = \overline{s't'}/\sigma_s\sigma_t$, where $\overline{s't'}$ is the covariance between two scalars, and $\sigma_s$and σ_t are their standard deviations, respectively. The random error in R_{st} is thus

$$\delta_{R_{st}} \approx \left[\delta_{\overline{s't'}}^2\left(\frac{\partial R_{st}}{\partial \overline{s't'}}\right)^2 + \delta_{\sigma_s}^2\left(\frac{\partial R_{st}}{\partial \sigma_s}\right)^2 + \delta_{\sigma_t}^2\left(\frac{\partial R_{st}}{\partial \sigma_t}\right)^2\right]^{\frac{1}{2}}, \tag{7a}$$

which can be simplified to

$$\delta_{R_{st}} \approx \left[\frac{\delta^2_{\overline{s't'}} \sigma_s^2 \sigma_t^2 + \sigma_t^2 \delta^2_{\sigma_s} \overline{s't'}^2 + \sigma_s^2 \delta^2_{\sigma_t} \overline{s't'}^2}{\sigma_s^4 \sigma_t^4} \right]^{\frac{1}{2}}. \tag{7b}$$

Another important indicator of scalar similarity is the relative transport efficiency of two scalars, defined as R_{ws}/R_{wt}. We note that there are many indicators of transport efficiency and the correlation coefficient between the vertical velocity and the scalar concentration (R_{ws}) is the one selected in our study. Hence the random error in the relative transport efficiency can be calculated from

$$\delta_{\frac{R_{ws}}{R_{wt}}} \approx \left[\delta^2_{R_{ws}} \left(\frac{1}{R_{wt}} \right)^2 + \delta^2_{R_{wt}} \left(\frac{-R_{ws}}{{R_{wt}}^2} \right)^2 \right]^{\frac{1}{2}} = \left[\frac{\delta^2_{R_{ws}} {R_{wt}}^2 + \delta^2_{R_{wt}} {R_{ws}}^2}{{R_{wt}}^4} \right]^{\frac{1}{2}}, \tag{8}$$

where the random errors $\delta_{R_{ws}}$ and $\delta_{R_{wt}}$ can be calculated using Eq. 7.

Once the random error is calculated, the relative random error (ε) is defined as the ratio of the random error to the absolute mean value.

2.2 Deriving Random Errors in C_s Using Monte-Carlo Simulations

So far, the random errors in all variables in the flux–variance relationship (Eq. 1) have been quantified except for C_s. Again, C_s is typically determined by linear regression between the measured $\sigma_s/|s_*|$ and $(-z/L)^{-1/3}$ over a range of strongly unstable conditions (Hsieh et al. 2008). As a result, it is difficult to find an explicit functional form to propagate errors from multiple $\sigma_s/|s_*|$ and $(-z/L)^{-1/3}$ data points to C_s. To quantify the influence of random errors on C_s, we propose a method based on Monte-Carlo simulations because of their wide use in uncertainty characterization in non-linear systems (Shen et al. 2013; Roy et al. 2014).

Given the values of $\sigma_s/|s_*|$ (and $-z/L$) and their uncertainties, a Gamma distribution is used to represent the distribution of $\sigma_s/|s_*|$ (and $-z/L$) for each 30-min segment. The mean of the Gamma distribution is assumed to be equal to the measured value, and the standard deviation is assumed to be equal to the random error. Ideally, Monte-Carlo samples should be drawn from the ensemble distributions; however, the actual ensemble distributions are inaccessible using our current datasets. Because both $\sigma_s/|s_*|$ and $-z/L$ are positive values with right-skewed distributions, we choose Gamma distributions instead of more commonly used symmetric distributions such as uniform, triangular, or Gaussian distributions (Shen et al. 2013; Roy et al. 2014). In support of this choice, we note that Gamma distributions have been widely used to model positive values with right-skewed distributions (Firth 1988; Dick 2004).

Once the distributions of $\sigma_s/|s_*|$ and $-z/L$ are determined, one value of $\sigma_s/|s_*|$ and one value of $-z/L$ can be randomly selected from their respective distributions for each 30-min segment. The collection of sampled values of $\sigma_s/|s_*|$ and $-z/L$ for all segments is thus one realization. A bi-square robust fitting algorithm is then applied to each realization to determine a value of C_s with the slope of the regression fixed to be '–1/3' on a log–log scale (Eq. 1). The above sampling and regression process is repeated 1000 times in order to obtain a representative distribution of C_s. A sensitivity study is performed to test the required number of realizations for statistical convergence, and results indicate that the difference between 1000 and 100,000 realizations is <1 %.

A threshold value ($-z/L = 0.1$) is chosen for regression as a compromise between including enough data for linear fitting and excluding data points that clearly do not follow the '$-1/3$' scaling. Previous studies such as Högström and Smedman-Högström (1974) and

Assouline et al. (2008) also used $-z/L = 0.1$ as the threshold, while Kader and Yaglom (1990) used an even smaller value of 0.04. In order to compare with other C_s values reported in previous studies, we choose to follow the typical way of obtaining C_s in these previous studies, that is, to fit a C_s value when the '$-1/3$' scaling appears in the data. As can be seen in our field data (shown later), the '$-1/3$' scaling occurs roughly when $-z/L > 0.1$.

It should be noted that the above method is completely different from the procedure used to test self-correlation as in Hartogensis and De Bruin (2005) and Cava et al. (2008), in which u_* (or scalar fluxes) are randomly shuffled for the whole dataset and are then used for calculating s_* and L. In their method, u_* (or scalar fluxes) entering into s_* and L have no relation to the truly measured u_* (or scalar fluxes). If a '$-1/3$' scaling still exists between $\sigma_s/|s_*|$ and $-z/L$ with randomly shuffled u_* (or scalar fluxes), it is an indication of self-correlation. In our method, the mean values of the distributions for $\sigma_s/|s_*|$ and $-z/L$ always remain the same and follow the '$-1/3$' scaling when $-z/L > 0.1$, and it is thus not surprising that the sampled data always follow the '$-1/3$' scaling as well when $-z/L > 0.1$.

3 Experimental Set-up and Data Processing

We conducted a field campaign at a commercial cattle feedlot in central Colorado, USA from November 12 to November 26 2013. The feedlot holds about 25,000 heads of cattle and the terrain is flat with a slope <5 %. The measurement system was deployed along the east edge of a block of pens and downwind of the prevailing westerly winds. The sampling area consisted mainly of feedlot pens holding cattle. An analytical footprint model was used to calculate the source area contributing to the flux measurements (Hsieh et al. 2000). The upwind distance that recovers 70 % of the flux was used as the fetch requirement, and only cases where a fetch inside the feedlot boundaries was used in the following analyses (Baum et al. 2008).

An open-path, QC laser-based NH_3 sensor was used to measure NH_3 concentration at 20 Hz. The sensor was described in detail previously (Miller et al. 2014) and it was calibrated by direct absorption spectroscopy before and after the field deployment. The instrument inaccuracy of NH_3 concentration is ± 10 %, and the instrument precision is $0.15\,\mu g\ m^{-3}$. Wind velocity and sonic temperature were measured using a three-dimensional sonic anemometer (CSAT3, Campbell Scientific, Inc., Logan, UT), while CO_2 and water vapour concentrations were measured using an open-path non-dispersive infrared (NDIR) gas sensor (LI-7500A, LI-COR Biosciences, Lincoln, Nebraska). The LI-7500A sensor was calibrated using the NOAA ESRL standard before and after the field deployment, all data logged at 20 Hz, with the LI-7500A instrument also measuring ambient pressure. All open-path sensors were mounted on a motorized tram attached to a tower at a height 4.92 m above ground; this measurement height had a fetch of 600 m for the prevailing westerly winds. Figure 1 shows the flux tower and the positions of the sonic anemometer, the CO_2 and H_2O combined sensor, and the NH_3 sensor.

The other dataset utilized for this study was collected over Lake Geneva in Switzerland during the summer and autumn of 2006. Measurements included wind velocity, temperature, and water vapour concentration at 20 Hz and at four different heights (1.65, 2.30, 2.95 and 3.60 m) above the lake surface. The details of this dataset have been described in previous studies (e.g., Bou-Zeid et al. 2008; Vercauteren et al. 2008; Li and Bou-Zeid 2011; Li et al. 2012).

Eddy-covariance (EC) data processing procedures and flux calculations have been described in detail previously by Li and Bou-Zeid (2011), who also used the same lake dataset. A brief summary is presented here, together with processing unique to NH_3 data in the feedlot dataset. Preprocessing included raw data despiking, double coordinate rotation,

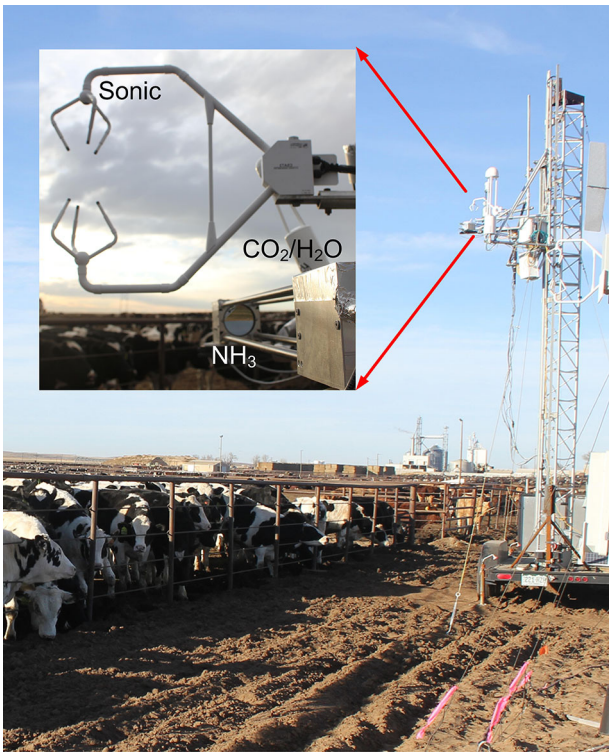

Fig. 1 Experimental set-up for the feedlot site. The *inset* gives a closer look at the sonic anemometer, the CO_2 and H_2O sensor, and the NH_3 sensor

and sonic temperature correction. The 20-Hz raw data of scalar concentrations were synchronized to the sonic wind data using the cross-covariance method. When calculating turbulent fluxes, an averaging period of 30 min was chosen, and the density corrections for NH_3, CO_2, and H_2O were applied (Webb et al. 1980). The self-heating effect of the LI-7500A was corrected following Burba et al. (2008). The spectroscopic effects of pressure, temperature, and water vapour fluctuations on NH_3 flux were corrected using a similar method for a commercial open-path methane analyzer, LI-7700 (McDermitt et al. 2011). The absorption line broadening effect caused by water vapour was quantified using line width data reported by Owen et al. (2013), where spectroscopic parameters of the same NH_3 absorption feature at 9.062 μm were measured experimentally. The high-frequency variance and covariance losses for trace gases due to sensor path-length integration and sensor separation were corrected using the theoretical transfer functions of Moore (1986). Highly non-stationary segments were excluded using the quality control described by Foken and Wichura (1996). The 30-min covariance between the vertical wind speed (w) and either the horizontal wind speed (u) or the scalar concentration (s) was compared to the averaged covariance of six consecutive 5-min blocks of data for the same 30-min period,

$$\Delta = \left| \frac{\left\langle \overline{w'a'}_5 \right\rangle - \overline{w'a'}_{30}}{\overline{w'a'}_{30}} \right|, \tag{9}$$

where a represents u or s, and the subscripts 5 and 30 denote the 5-min and the 30-min covariance, respectively. The bracket denotes the mean of the six 5-min covariances. Periods

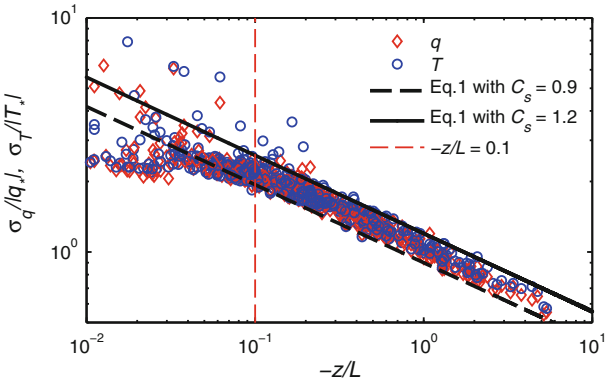

Fig. 2 Flux–variance relationships for temperature (T) and water vapour (q) under unstable conditions from the lake dataset. The *two black lines* represent Eq. 1 with $C_s = 0.9$ and 1.2, respectively. The *vertical dashed red line* denotes $-z/L = 0.1$ where the '$-1/3$' scaling starts to appear

in which $\Delta > 30\,\%$ for u or any scalar s were considered highly non-stationary and excluded in our analyses.

4 Results

4.1 Random Errors in C_s in Flux–Variance Relationships

Flux–variance relationships for temperature (T) and water vapour (q) from the lake dataset are presented in Fig. 2; Eq. 1 with C_s of 0.9 and 1.2 is also shown in order to illustrate the typical range of C_s. As can be seen, the flux–variance relationships for both temperature and water vapour approach a slope of '$-1/3$' in the log–log plot when $-z/L > 0.1$. Under such conditions, most data points lie between the two asymptotic lines represented by Eq. 1 with $C_s = 0.9$ and 1.2, implying that the values of both C_T and C_q determined from this dataset lie between 0.9 and 1.2. This is consistent with the range of C_s reported in the literature from 0.9 to 1.4 (Monin and Yaglom 1975; Asanuma and Brutsaert 1999; Assouline et al. 2008; Hsieh et al. 2008). Nonetheless, most previous studies either completely neglected the uncertainty in C_s or only reported the uncertainty resulting from the fitting procedure but ignored the uncertainty resulting from the random errors associated with $-z/L$ and $\sigma_s/|s_*|$. Our aim here is to quantify the impacts of random errors in turbulence measurements on the uncertainty in C_s. To do so, we need to first understand the random errors in $-z/L$ and $\sigma_s/|s_*|$.

The random errors in $-z/L$ are calculated using Eq. 6 and displayed in Fig. 3. As can be seen, the relative random errors in $-z/L$ do not show any significant dependence on measurement heights in the lake dataset and they increase with instability in both datasets, mainly because they are proportional to $1/u_*^3$, and $u_* \to 0$ in the free convection limit (Salesky and Chamecki 2012). They also show a similar pattern in the two datasets, although the lake dataset covers a wider range of $-z/L$.

Similarly, random errors in different $\sigma_s/|s_*|$ were calculated based on Eq. 5. We use the variable c to denote CO_2 concentration and the symbol r to denote NH_3 concentration. The relative random errors in $\sigma_T/|T_*|$ and $\sigma_q/|q_*|$ calculated from both datasets are shown in

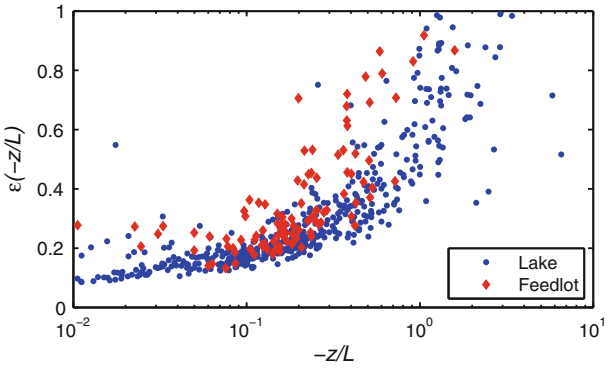

Fig. 3 Relative random errors in $-z/L$

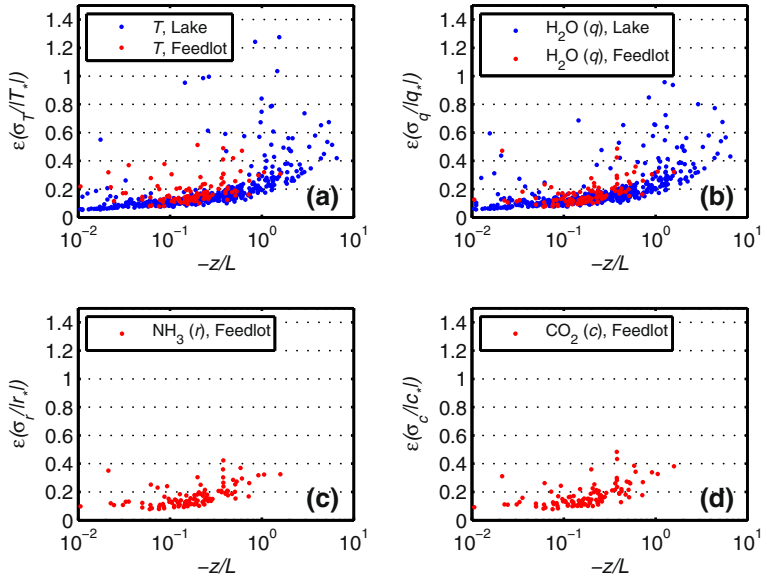

Fig. 4 Relative random errors in $\sigma_s/|s_*|$

Fig. 4a, b, and the relative random errors in $\sigma_r/|r_*|$ and $\sigma_c/|c_*|$ from the feedlot dataset are shown in Fig. 4c, d. For both datasets, the relative random errors in $\sigma_s/|s_*|$ are typically on the order of 10–20 % under near-neutral to moderately unstable conditions and they increase with instability. The large relative errors in $-z/L$ under strongly unstable conditions shown in Fig. 3 are likely the major cause of large scatter seen in Fig. 4, as discussed in Salesky and Chamecki (2012).

With the calculated random errors in $-z/L$ (Fig. 3) and $\sigma_s/|s_*|$ (Fig. 4), error bars can now be included in flux–variance relationships, as shown in Fig. 5. The horizontal error bars represent random errors in $-z/L$ and the vertical error bars represent random errors in $\sigma_s/|s_*|$. Most data in Fig. 5a–f show that when $-z/L > 0.1$, $\sigma_s/|s_*|$ follows a linear relationship with $-z/L$ using a log–log scale. The outliers generally have large errors in both $\sigma_s/|s_*|$ and $-z/L$.

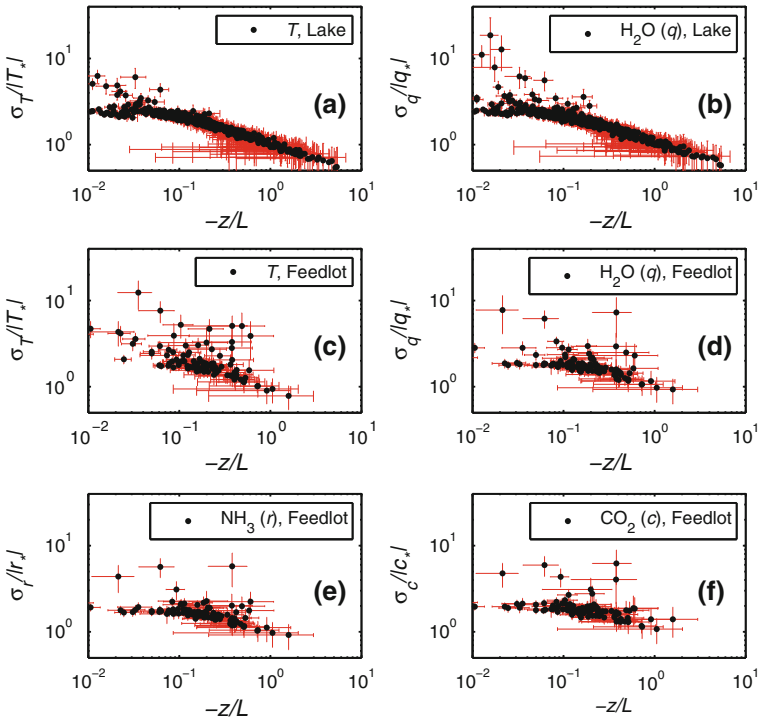

Fig. 5 Flux–variance relationships for different scalars under unstable conditions from the lake dataset (**a**, **b**) and the feedlot dataset (**c–f**). *Error bars* indicate uncertainties resulting from random errors in turbulence measurements

As mentioned earlier, C_s in the flux–variance relationship (Eq. 1) was traditionally determined by linear regression between measured $\sigma_s/|s_*|$ and $(-z/L)^{-1/3}$ over a range of strongly unstable conditions (Hsieh et al. 2008). Such a simple regression method provides equal weight to all the data points regardless of their errors. Therefore, simple regression results are strongly influenced by outliers with large errors (see Fig. 5). In addition, such a simple regression method cannot properly quantify the uncertainties in C_s.

As discussed in Sect. 2.2, a method based on Monte-Carlo simulations is proposed to quantify the uncertainties in C_s. Figure 6 shows an example of using the Monte-Carlo sampling method to quantify the uncertainty in C_q in the lake dataset. In each of the four realizations shown in the four different panels, paired samples of $\sigma_q/|q_*|$ and $-z/L$ are randomly drawn from their respective Gamma distributions for each 30-min segment and a value of C_q is then obtained through a bi-square fitting. With 1000 realizations, the Monte-Carlo method therefore produces a distribution of C_q, which can be then used to characterize the uncertainty in C_q caused by random errors in turbulence measurements, as shown in Figs. 7 and 8.

Figure 7a and b shows the distributions of C_T and C_q from the lake dataset, and Fig. 7c–f shows the distributions of C_T, C_q, C_r and C_c from the feedlot dataset. The mean values of C_s, shown in the legend, are similar for different scalars and across the two datasets with values ranging from 1.00 to 1.05. Also shown are the 95 % confidence intervals of the mean values. The majority of C_s values range from 0.9 to 1.1, in agreement with previous estimates (Monin and Yaglom 1975; Asanuma and Brutsaert 1999; Assouline et al. 2008; Hsieh et al. 2008). Figure 8 further shows that the distributions of C_s significantly overlap among different

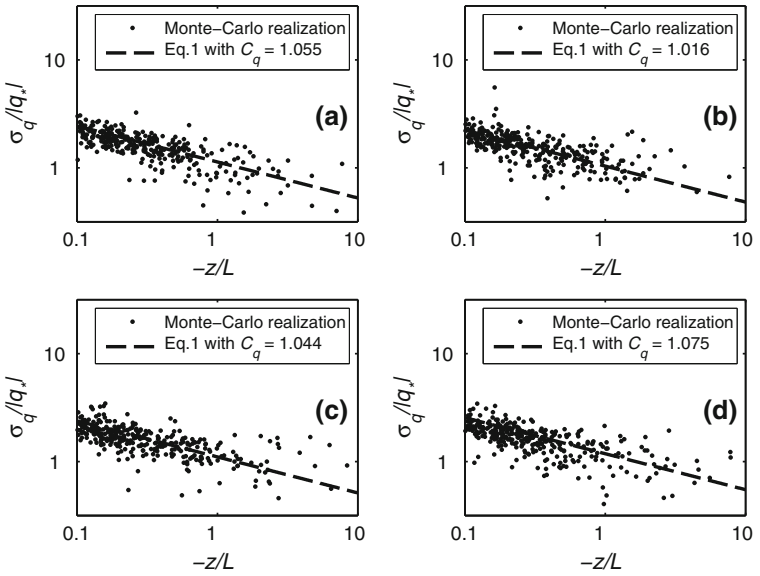

Fig. 6 An example of using the Monte Carlo method to determine C_q in the lake dataset. Four realizations with different fitted C_q values are shown in the four panels

scalars in both datasets, despite the vastly different measurement environments, implying that these scalars are transported similarly under strongly unstable conditions at the two sites. In particular, temperature does not show significant deviations from the other scalars due to its 'active role' under unstable conditions (Katul and Parlange 1994; Katul and Hsieh 1999).

The flux–variance relationship of NH_3 requires further discussion. The NH_3 sensor size is 0.7 m (Miller et al. 2014), which is significantly larger than that of the water vapour and CO_2 sensor (0.125 m). It is critical to correct high-frequency variance and covariance losses for NH_3 due to the sensor path-length integration. These corrections are generally <1 % for water vapour and CO_2 but can be up to 10 % for NH_3. Because high-frequency losses are larger in the variance than in the covariance, neglecting the high-frequency loss correction will significantly underestimate C_r. For example, the mean value of C_r without high-frequency loss corrections would have been 0.96 (as compared to 1.00 shown in Fig. 7e) if the high-frequency loss corrections were not applied.

4.2 Random Errors in R_{st} and R_{ws}/R_{wt}

The random errors in two other important measures of scalar similarity, the correlation coefficient between two scalars (R_{st}) and the relative transport efficiency (R_{ws}/R_{wt}), are also quantified using the feedlot dataset. Unlike C_s, which only exists under strongly unstable conditions, these two measures of scalar similarity exist under both stable and unstable conditions. Temperature is excluded from this analysis due to its self-correlation with z/L.

As shown in Fig. 9, the relative random errors in the correlation coefficients increase when the ASL departs from neutral conditions. These relative random errors are <10 % under near-neutral conditions and increase to around 20 % under very stable or unstable conditions. The increases in relative random errors are primarily due to increases in the random errors themselves rather than decreases in the correlation coefficients. This suggests

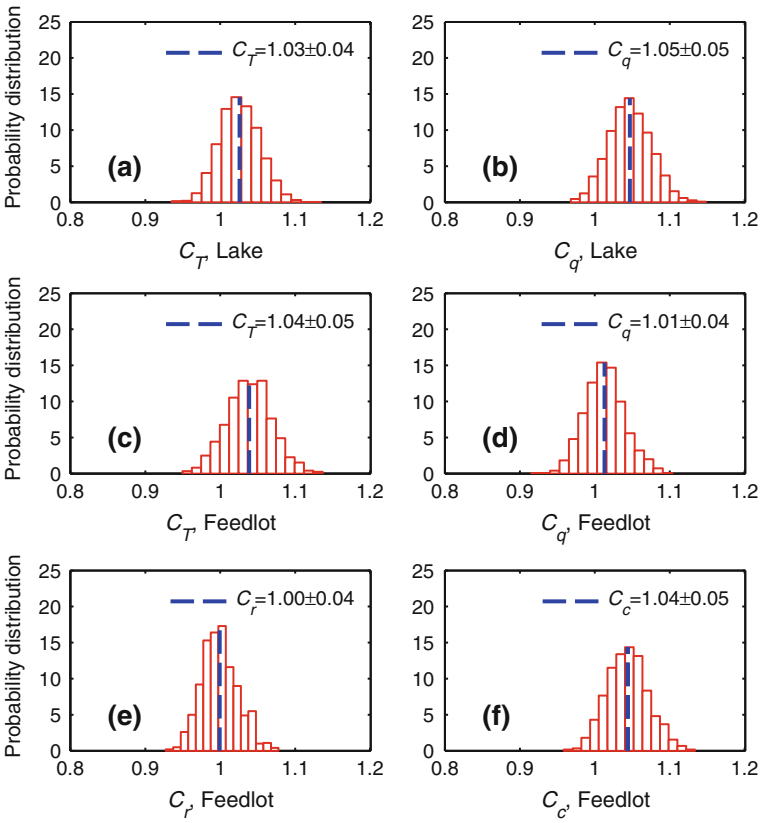

Fig. 7 The distributions of C_T (**a**) and C_q (**b**) from the lake dataset, and C_T (**c**), C_q (**d**), C_r (**e**) and C_c (**f**) from the feedlot dataset derived from 1000 Monte-Carlo simulations. The mean and 95 % confidence interval values are also shown

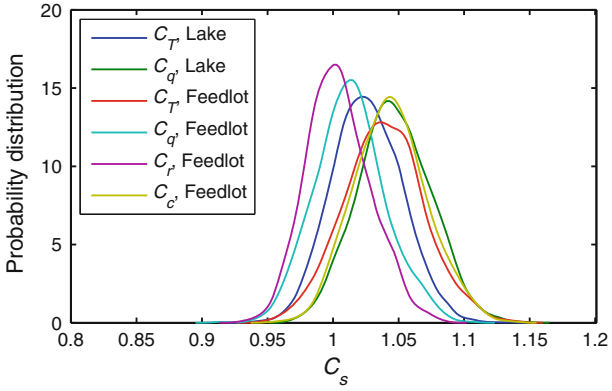

Fig. 8 Smoothed probability density distributions of C_s for different scalars in both lake and feedlot datasets

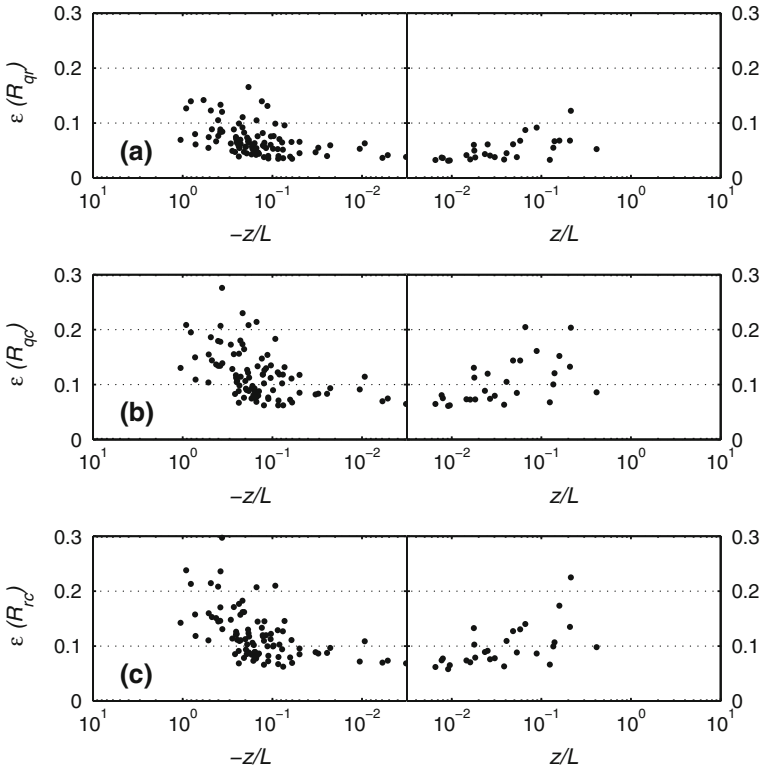

Fig. 9 Relative random errors in the correlation coefficients between water vapour and NH_3 (**a**), water vapour and CO_2 (**b**), and CO_2 and NH_3 (**c**) from the feedlot dataset

that there might be significant random errors associated with the correlation coefficients under strongly unstable and stable conditions. As a result, their random errors should be quantified before using them as indicators for scalar similarity.

In Fig. 10, the correlation coefficients between water vapour, NH_3, and CO_2 are shown as a function of z/L with their random errors displayed as vertical error bars. The correlation coefficients are generally large ($R_{qr} = 0.87 \pm 0.10$; $R_{qc} = 0.89 \pm 0.11$; $R_{rc} = 0.89 \pm 0.04$) and do not show a significant dependence on z/L. This is because the sources of water vapour, NH_3, and CO_2 are all related to animal activities in the feedlot and thus are well co-located. It is interesting to note that the correlation coefficients that include q are small for some unstable segments, whereas this does not occur for R_{rc}. Close inspection reveals that these low values of correlation coefficients including q primarily occurred after a strong snowstorm. As a result, the water vapour flux was due to the snow in these periods whereas the NH_3 and CO_2 fluxes were still mainly biogenic. This may explain the small correlations between water vapour and NH_3/CO_2 under such conditions.

There are many data points that reach a value of unity when the random errors are considered. If the random errors were not quantified, these data points would have indicated dissimilarity between scalars. The scalar similarity of the entire dataset is further investigated by a χ^2 test with the null hypothesis of $R_{st} = 1$. Here the test statistic $\chi^2 = \sum_N \left(\frac{R_{st}-1}{\delta_{R_{st}}}\right)^2$ is compared to a χ^2 distribution with N degrees of freedom, where $N = 99$ is the number of 30-min segments. The values of statistic $\chi^2(N = 99)$ are 353, 269, and 168 for R_{qr}, R_{qc},

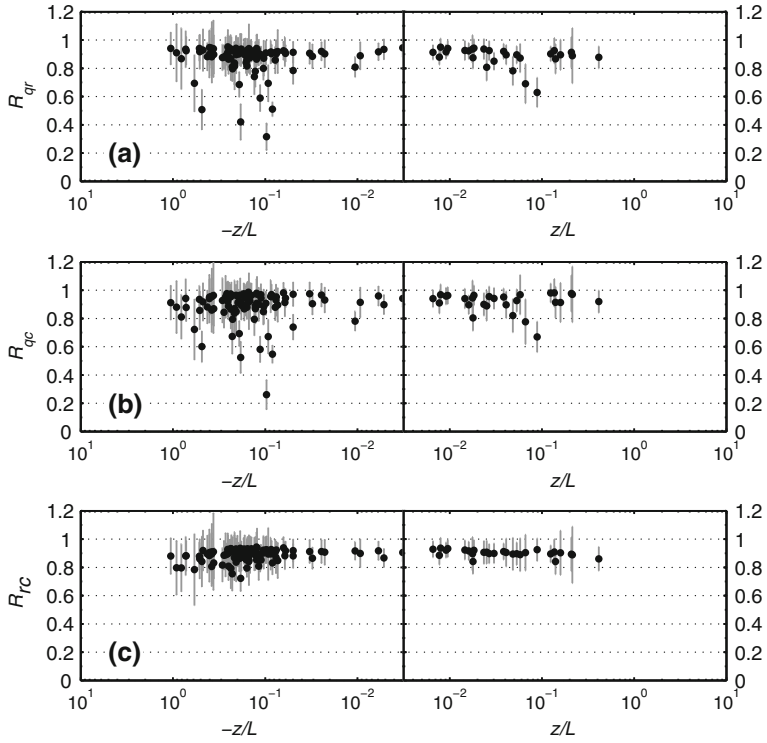

Fig. 10 Correlation coefficients between water vapour and NH_3 (**a**), water vapour and CO_2 (**b**), and CO_2 and NH_3 (**c**) from the feedlot dataset. The random errors are displayed as *vertical error bars*

and R_{rc}, respectively, and the associated probability of falsely rejecting the null hypothesis is much less than 0.001 in all three cases. Therefore, the χ^2 test suggests that the null hypothesis can be rejected at a high (>99.9 %) confidence level, implying that scalar similarity does not hold across the entire dataset.

We further investigate the relative random errors in the relative transport efficiencies (R_{ws}/R_{wt}, where s, t are two scalars). Note the relative transport efficiencies (R_{ws}/R_{wt}) are asymmetric for s and t, and a symmetric relative transport efficiency has been proposed elsewhere (Cancelli et al. 2012) but is not used here. As can be seen from Fig. 11, the relative random errors in the relative transport efficiencies also increase as the atmosphere departs from neutral conditions and reach 30 % under strongly unstable and stable conditions. This again highlights the need to quantify the random errors associated with the relative transport efficiencies.

The relative transport efficiencies are also shown as a function of z/L in Fig. 12 where most of the data are clustered around unity consistent with Fig. 10. Many data points can no longer be distinguished from unity when the random errors are considered, implying that no judgment can be made about scalar dissimilarity under such conditions. A similar χ^2 test is performed with the null hypothesis of $R_{ws}/R_{wt} = 1$. Here the test statistic is $\chi^2 = \sum_N \left(\frac{R_{ws}/R_{wt}-1}{\delta \frac{R_{ws}}{R_{wt}}} \right)^2$. The values of statistic $\chi^2(N = 99)$ are 76, 59, and 63 for R_{wq}/R_{wr}, R_{wq}/R_{wc}, and R_{wr}/R_{wc}, respectively, and thus the associated probability of falsely rejecting the null hypothesis is >0.1 in all three cases, implying that the null hypothe-

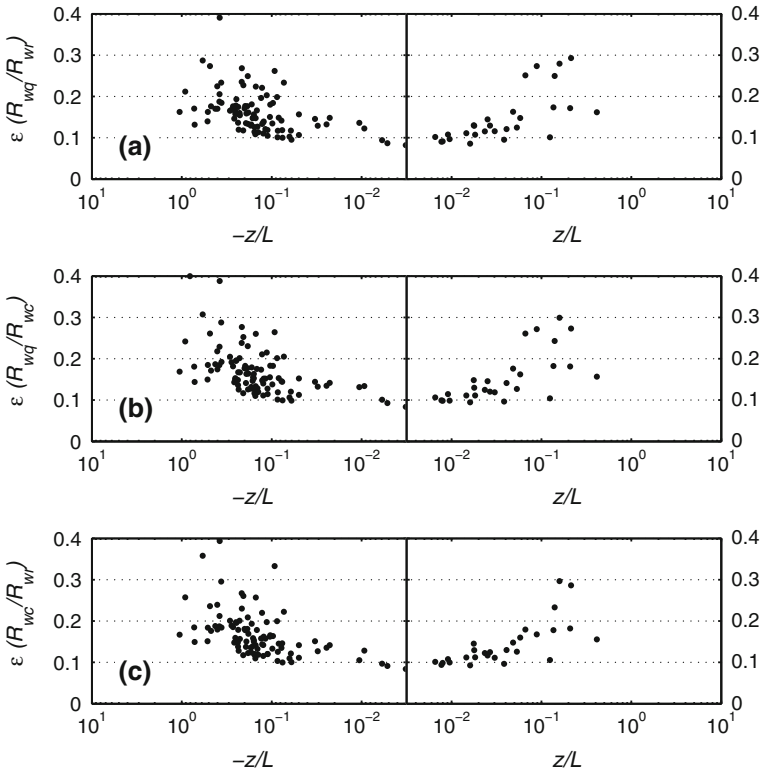

Fig. 11 Relative random errors in relative transport efficiencies between water vapour and NH_3 (**a**), water vapour and CO_2 (**b**), and CO_2 and NH_3 (**c**) from the feedlot dataset

sis cannot be rejected even at a relatively low confidence level of 90 %. In other words, scalar similarity is supported by the relative transport efficiencies across the entire dataset. Given that $R_{wt}/R_{ws} = C_s/C_t$ for any two scalars s and t, the finding that R_{wt}/R_{ws} is not statistically different from unity for water vapour, NH_3, and CO_2 is consistent with our previous finding that their mean values of C_s are similar (see Fig. 8).

The comparison between correlation coefficients and relative transport efficiencies shows interesting differences between the two measures of scalar similarity. In the feedlot dataset, the correlation coefficients among the three scalars (water vapour, CO_2, and NH_3) are statistically different from unity while the relative transport efficiencies are not, consistent with the finding of Cancelli et al. (2012) that the relative transport efficiencies were usually larger than the correlation coefficients in their lake data. Cancelli et al. (2012) argued that the correlation coefficients represent more the *scalar similarity* but the relative transport efficiencies represent more the *scalar flux similarity*. One should also note that the correlation coefficients are bounded by unity, while the relative transport efficiencies can be either larger or smaller than unity. Hence, it is naturally more difficult for the correlation coefficients to be statistically identical to unity.

The relationship between R_{st} and R_{ws}/R_{wt} has been discussed in many previous studies (e.g., Katul et al. 1995; Bink and Meesters 1997; Katul and Hsieh 1997; Lamaud and Irvine 2006; Guo et al. 2009; Dias 2013); however, there is no consensus on the exact relationship

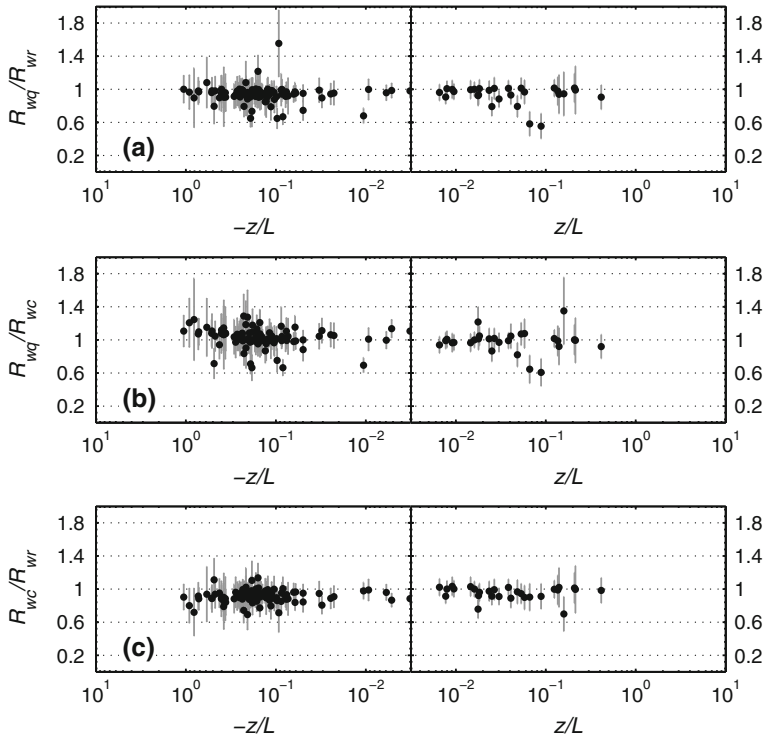

Fig. 12 Relative transport efficiencies between water vapour and NH_3 (**a**), water vapour and CO_2 (**b**), and CO_2 and NH_3 (**c**) from the feedlot dataset. The random errors are displayed as *vertical error bars*

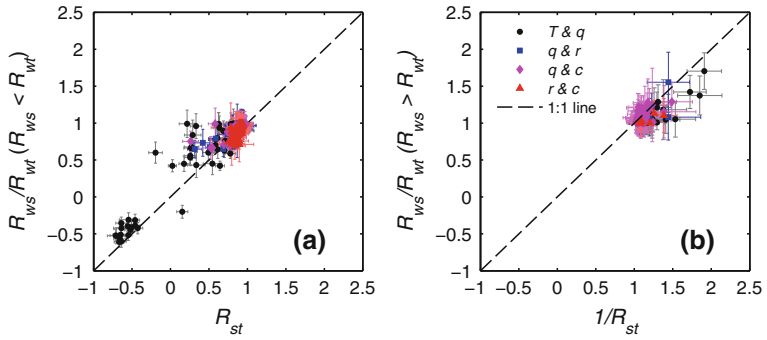

Fig. 13 The relationship between R_{st} and R_{ws}/R_{wt} when the random errors are considered. **a** R_{st} is on the x-axis and only $R_{ws}/R_{wt} < 1$ are shown on the y-axis. **b** $1/R_{st}$ is on the x-axis and only $R_{ws}/R_{wt} > 1$ are shown on the y-axis

between the two (Lamaud and Irvine 2006; Guo et al. 2009). When their random errors are considered, the relationship between the two measures of scalar similarity becomes more complicated, as shown in Fig. 13. Note since z/L is not shown here, temperature is also included in the figure.

Figure 13 shows that most of the data points follow the 1:1 line ($R^2 = 0.81$), supporting using one as a surrogate for the other to estimate turbulent fluxes as done in many previous

studies (Katul et al. 1995, 1996). Note that R_{st} is plotted against R_{ws}/R_{wt} when $R_{ws}/R_{wt} < 1$, whereas $1/R_{st}$ is plotted against R_{ws}/R_{wt} when $R_{ws}/R_{wt} > 1$. The random errors in these measures, when added to the figure, contribute to the scatter. In particular, it is sometimes difficult to distinguish the dry cases ($R_{wT} > R_{wq}$) from the wet cases ($R_{wT} < R_{wq}$) as in Bink and Meesters (1997) when these large error bars are considered. These large error bars might also partly explain why Guo et al. (2009) obtained a different relationship between $\log_{10}(R_{wT}/R_{wq})/\log_{10}(R_{qT})$ and the Bowen ratio as compared to Lamaud and Irvine (2006).

5 Conclusion and Discussion

We investigate the influence of random errors in turbulence measurements on scalar similarity using two datasets (collected over a lake and a feedlot) and multiple scalars (temperature, water vapour, CO_2, and NH_3). The random errors in the similarity constant C_s in the flux–variance relationship are quantified based on error propagation analyses and Monte-Carlo simulations. For each scalar, a distribution of C_s, instead of a single value as was usually reported in previous experimental studies, is obtained when random errors in turbulence measurements are considered. It is found that, although the distributions of C_s for different scalars are not identical, the differences among the mean values of C_s ($\approx$0.05) are well within the 95 % confidence intervals of C_s ($\approx$0.1). This implies that the scalars are transported similarly under strongly unstable conditions at these two sites.

The random errors in the correlation coefficients and the relative turbulent transport efficiencies are also investigated using the feedlot dataset. The correlation coefficients among three scalars (water vapour, CO_2, and NH_3) are high ($R_{qr} = 0.87 \pm 0.10$; $R_{qc} = 0.89 \pm 0.11$; $R_{rc} = 0.89 \pm 0.04$) and do not show any significant dependence on atmospheric stability. The relative transport efficiencies are all clustered around unity and also do not show a dependence on z/L. However, their relative random errors both increase as the atmosphere departs from neutral conditions, reaching 30–40 % under strongly stratified conditions. When their random errors are considered, it is further observed that these two measures of scalar similarity are not different from unity for some data points. To rigorously assess scalar similarity using these two measures across the whole dataset, statistical tests (the χ^2 test) are conducted. The correlation coefficients among three scalars are statistically different from unity while the relative transport efficiencies are not. This highlights the difference between the correlation coefficients and the relative transport efficiencies, as they represent *scalar similarity* and *scalar flux similarity*, respectively (Bink and Meesters 1997; Katul and Hsieh 1997; Cancelli et al. 2012; Dias 2013), and the correlation coefficients are bounded by unity while the relative transport efficiencies are not. The random errors also complicate the relationship between correlation coefficients and the relative transport efficiencies, which might explain why different relationships between $\log_{10}(R_{wT}/R_{wq})/\log_{10}(R_{qT})$ and the Bowen ratio have been reported in different studies (Lamaud and Irvine 2006; Guo et al. 2009). Furthermore, the finding that the relative transport efficiencies are not statistically different from unity for the three scalars is consistent with the finding that their mean values of C_s are also similar given $C_s/C_t = R_{wt}/R_{ws}$.

The results highlight the importance of assessing the impacts of random errors in turbulence measurements on three measures of scalar similarity: the similarity constant in the flux–variance relationship, the correlation coefficient between two scalars, and the relative transport efficiency. In particular, the datasets used in our study were collected over relatively homogenous and flat surfaces, that is, under 'near-ideal' conditions. As a result, our conclusions might be specific to these two measurement environments. However, given that we

have already observed important impacts of random errors on measures of scalar similarity under these 'near-ideal' conditions, it is recommended that the random errors should always be considered when comparing indicators for scalar similarity.

It is acknowledged that, although the non-stationarity effects have been minimized by imposing the quality control (i.e., Δ calculated by Eq. 9 should be <30 %), the data might still include residual non-stationarity effects. Since truly stationary time series rarely occur in the ASL, it is difficult to completely exclude non-stationarity effects. Future studies using highly stationary measurements, for example from controlled laboratory experiments, are recommended.

Acknowledgments The authors acknowledge the research group of Azer Yalin at Colorado State University for providing laboratory space and Jay Ham, Kira Shonkwiler, Christina Nash for the set-up and operation of the tower at the feedlot site. The feedlot work was supported by the Center for Mid-Infrared Technologies for Health and the Environment (MIRTHE) under National Science Foundation Grant No. EEC-0540832. Kang Sun acknowledges support by a NASA Earth and Space Science Fellowship (NN12AN64H). Dan Li acknowledges support from the NOAA (U.S. Department of Commerce) Grant NA08OAR4320752 and the Carbon Mitigation Initiative at Princeton University, sponsored by British Petroleum. Zhongkuo Zhao acknowledges support from the Strategic Priority Research Program of the Chinese Academy of Sciences (Grant No. XDA11010403). The statements, findings, and conclusions are those of the authors and do not necessarily reflect the views of the NOAA, the U.S. Department of Commerce or British Petroleum. The lake dataset was kindly provided by the Environmental Fluid Mechanics and Hydrology Laboratory of Prof. Marc Parlange at The École polytechnique fédérale de Lausanne.

References

Asanuma J, Brutsaert W (1999) Turbulence variance characteristics of temperature and humidity in the unstable atmospheric surface layer above a variable pine forest. Water Resour Res 35:515–521. doi:10.1029/1998wr900051

Asanuma J, Tamagawa I, Ishikawa H, Ma Y, Hayashi T, Qi Y, Wang J (2007) Spectral similarity between scalars at very low frequencies in the unstable atmospheric surface layer over the Tibetan plateau. Boundary-Layer Meteorol 122:85–103. doi:10.1007/s10546-006-9096-y

Assouline S, Tyler SW, Tanny J, Cohen S, Bou-Zeid E, Parlange M, Katul G (2008) Evaporation from three water bodies of different sizes and climates: measurements and scaling analysis. Adv Water Resour 31:160–172. doi:10.1016/j.advwatres.2007.07.003

Baum KA, Ham JM, Brunsell NA, Coyne PI (2008) Surface boundary layer of cattle feedlots: implications for air emissions measurement. Agric For Meteorol 148:1882–1893. doi:10.1016/j.agrformet.2008.06.017

Bink NJ, Meesters A (1997) Comment on "Estimation of surface heat and momentum fluxes using the flux-variance method above uniform and non-uniform terrain" by Katul et al. (1995). Boundary-Layer Meteorol 84:497–502

Bou-Zeid E, Vercauteren N, Parlange MB, Meneveau C (2008) Scale dependence of subgrid-scale model coefficients: an a priori study. Phys Fluids 20:115106

Brutsaert W (1982) Evaporation into the atmosphere: theory, history, and applications. Reidel, Dordrecht, 299 pp

Burba G, Mcdermitt DK, Grelle A, Anderson D, Xu L (2008) Addressing the influence of instrument surface heat exchange on the measurements of CO_2 flux from open-path gas analyzers. Glob Chang Biol 14:1854–1876. doi:10.1111/j.1365-2486.2008.01606.x

Cancelli DM, Dias NL, Chamecki M (2012) Dimensionless criteria for the production-dissipation equilibrium of scalar fluctuations and their implications for scalar similarity. Water Resour Res. doi:10.1029/2012WR012127

Cava D, Katul G, Sempreviva AM, Giostra U, Scrimieri A (2008) On the anomalous behaviour of scalar flux-variance similarity functions within the canopy sub-layer of a dense alpine forest. Boundary-Layer Meteorol 128:33–57. doi:10.1007/s10546-008-9276-z

De Bruin HAR, Van Den Hurk B, Kroon LJM (1999) On the temperature-humidity correlation and similarity. Boundary-Layer Meteorol 93:453–468

Detto M, Katul G, Mancini M, Montaldo N, Albertson J (2008) Surface heterogeneity and its signature in higher-order scalar similarity relationships. Agric For Meteorol 148:902–916. doi:10.1016/j.agrformet.2007.12.008

Dias NL (2013) Research on atmospheric turbulence by Wilfried Brutsaert and collaborators. Water Resour Res 49:7169–7184

Dias NL, Brutsaert W (1996) Similarity of scalars under stable conditions. Boundary-Layer Meteorol 80:355–373

Dick EJ (2004) Beyond "lognormal versus gamma": discrimination among error distributions for generalized linear models. Fish Res 70:351–366

Firth D (1988) Multiplicative errors: log-normal or gamma? J R Stat Soc Ser B 50:266–268

Foken T, Wichura B (1996) Tools for quality assessment of surface-based flux measurements. Agric For Meteorol 78:83–105. doi:10.1016/0168-1923(95)02248-1

Guo X, Zhang H, Cai X, Kang L, Zhu T, Leclerc M (2009) Flux-variance method for latent heat and carbon dioxide fluxes in unstable conditions. Boundary-Layer Meteorol 131:363–384. doi:10.1007/s10546-009-9377-3

Hartogensis OK, De Bruin HAR (2005) Monin–Obukhov similarity functions of the structure parameter of temperature and turbulent kinetic energy dissipation rate in the stable boundary layer. Boundary-Layer Meteorol 116:253–276. doi:10.1007/s10546-004-2817-1

Hill RJ (1989) Implications of Monin–Obukhov similarity theory for scalar quantities. J Atmos Sci 46:2236–2244

Högström U, Smedman-Högström A-S (1974) Turbulence mechanisms at an agricultural site. Boundary-Layer Meteorol 7:373–389

Hsieh C, Katul G, Chi T (2000) An approximate analytical model for footprint estimation of scalar fluxes in thermally stratified atmospheric flows. Adv Water Resour 23:765–772

Hsieh C-I, Lai M-C, Hsia Y-J, Chang T-J (2008) Estimation of sensible heat, water vapor, and CO_2 fluxes using the flux-variance method. Int J Biometeorol 52:521–533. doi:10.1007/s00484-008-0149-4

Kader BA, Yaglom AM (1990) Mean fields and fluctuation moments in unstably stratified turbulent boundary layers. J Fluid Mech 212:637–662

Katul G, Goltz SM, Hsieh C-I, Cheng Y, Mowry F, Sigmon J (1995) Estimation of surface heat and momentum fluxes using the flux-variance method above uniform and non-uniform terrain. Boundary-Layer Meteorol 74:237–260

Katul G, Hsieh C-I (1997) Reply to the comment by Bink and Meesters. Boundary-Layer Meteorol 84:503–509

Katul G, Hsieh C-I, Oren R, Ellsworth D, Phillips N (1996) Latent and sensible heat flux predictions from a uniform pine forest using surface renewal and flux variance methods. Boundary-Layer Meteorol 80:249–282

Katul G, Hsieh C-I (1999) A note on the flux-variance similarity relationships for heat and water vapour in the unstable atmospheric surface layer. Boundary-Layer Meteorol 90:327–338

Katul G, Parlange MB (1994) On the active role of temperature in surface-layer turbulence. J Atmos Sci 51:2181–2195

Katul G, Sempreviva AM, Cava D (2008) The temperature-humidity covariance in the marine surface layer: a one-dimensional analytical model. Boundary-Layer Meteorol 126:263–278. doi:10.1007/s10546-007-9236-z

Lamaud E, Irvine M (2006) Temperature-humidity dissimilarity and heat-to-water-vapour transport efficiency above and within a pine forest canopy: the role of the Bowen ratio. Boundary-Layer Meteorol 120:87–109

Lee X, Yu Q, Sun X, Liu J, Min Q, Liu Y, Zhang X (2004) Micrometeorological fluxes under the influence of regional and local advection: a revisit. Agric For Meteorol 122:111–124

Li D, Bou-Zeid E (2011) Coherent structures and the dissimilarity of turbulent transport of momentum and scalars in the unstable atmospheric surface layer. Boundary-Layer Meteorol 140:243–262. doi:10.1007/s10546-011-9613-5

Li D, Bou-Zeid E, De Bruin HAR (2012) Monin–Obukhov similarity functions for the structure parameters of temperature and humidity. Boundary-Layer Meteorol 145:45–67. doi:10.1007/s10546-011-9660-y

Lumley JL, Panofsky HA (1964) The structure of atmospheric turbulence. Interscience Publishers, New York, 239 pp

Martin ST, Hung H-M, Park RJ, Jacob D, Spurr R, Chance K, Chin M (2004) Effects of the physical state of tropospheric ammonium-sulfate-nitrate particles on global aerosol direct radiative forcing. Atmos Chem Phys 4:183–214

McDermitt D, Burba G, Xu L, Anderson T, Komissarov A, Riensche B, Schedlbauer J, Starr G, Zona D, Oechel W, Oberbauer S, Hastings S (2011) A new low-power, open-path instrument for measuring methane flux by eddy covariance. Appl Phys B 102:391–405

McNaughton KG, Laubach J (1998) Unsteadiness as a cause of non-equality of eddy diffusivities for heat and vapour at the base of an advective inversion. Boundary-Layer Meteorol 88:479–504

Miller DJ, Sun K, Tao L, A Khan, Zondlo M (2014) Open-path, quantum cascade-laser-based sensor for high-resolution atmospheric ammonia measurements. Atmos Meas Tech 7:81–93. doi:10.5194/amt-7-81-2014

Moene AF, Schuttemeyer D (2008) The effect of surface heterogeneity on the temperature-humidity correlation and the relative transport efficiency. Boundary-Layer Meteorol 129:99–113. doi:10.1007/s10546-008-9312-z

Monin AS, Obukhov AM (1954) Basic laws of turbulent mixing in the ground layer of the atmosphere. Akad Nauk SSSR, Geofiz Inst Tr 151:163–187

Monin AS, Yaglom AM (1975) Statistical fluid mechanics. MIT Press, Cambridge, 874 pp

Moore CJ (1986) Frequency response corrections for eddy correlation systems. Boundary-Layer Meteorol 37:17–35. doi:10.1007/BF00122754

Owen K, Es-sebbar E, Farooq A (2013) Measurements of NH_3 linestrengths and collisional broadening coefficients in N_2, O_2, CO_2, and H_2O near 1103.46cm^{-1}. J Quant Spectrosc Radiat Transf 121:56–68. doi:10.1016/j.jqsrt.2013.02.001

Roy AA, Adams PJ, Robinson AL (2014) Air pollutant emissions from the development, production, and processing of Marcellus Shale natural gas. J Air Waste Manage Assoc 64:19–37

Salesky ST, Chamecki M (2012) Random errors in turbulence measurements in the atmospheric surface layer: implications for Monin–Obukhov similarity theory. J Atmos Sci 69:3700–3714. doi:10.1175/JAS-D-12-096.1

Salesky ST, Chamecki M, Dias NL (2012) Estimating the random error in eddy-covariance based fluxes and other turbulence statistics: the filtering method. Boundary-Layer Meteorol 144:113–135. doi:10.1007/s10546-012-9710-0

Sempreviva AM, Hojstrup J (1998) Transport of temperature and humidity variance and covariance in the marine surface layer. Boundary-Layer Meteorol 87:233–253

Shen H, Huang Y, Wang R, Zhu D, Li W, Shen G, Wang B, Zhang Y, Chen Y, Lu Y, Chen H, Li T, Sun K, Li B, Liu W, Liu J, Tao S (2013) Global atmospheric emissions of polycyclic aromatic hydrocarbons from 1960 to 2008 and future predictions. Environ Sci Technol 47:6415–6424. doi:10.1021/es400857z

Shindell DT, Faluvegi G, Koch DM, Schmidt GA, Unger N, Bauer SE (2009) Improved attribution of climate forcing to emissions. Science 326:716–718. doi:10.1126/science.1174760

Stensrud DJ (2007) Parameterization schemes: keys to understanding numerical weather prediction models. Cambridge University Press, Cambridge, 459 pp

Stull RB (1988) An introduction to boundary layer meteorology. Kluwer Academic Publishers, Dordrecht, 666 pp

Sun K, Tao L, Miller DJ, Khan M, Zondlo M (2014) On-road ammonia emissions characterized by mobile, open-path measurements. Environ Sci Technol 48:3943–3950. doi:10.1021/es4047704

Vercauteren N, Bou-Zeid E, Parlange MB, Lemmin U, Huwald H, Selker J, Meneveau C (2008) Subgrid-scale dynamics of water vapour, heat, and momentum over a lake. Boundary-Layer Meteorol 128:205–228. doi:10.1007/s10546-008-9287-9

Webb EK, Pearman GI, Leuning R (1980) Correction of flux measurements for density effects due to heat and water vapour transfer. Q J R Meteorol Soc 106:85–100

Williams CA, Scanlon TM, Albertson JD (2007) Influence of surface heterogeneity on scalar dissimilarity in the roughness sublayer. Boundary-Layer Meteorol 122:149–165

Zhao Z, Gao Z, Li D, Bi X, Liu C, Liao F (2013) Scalar flux-gradient relationships under unstable conditions over water in coastal regions. Boundary-Layer Meteorol 148:495–516. doi:10.1007/s10546-013-9829-7